Dynamic analysis of DC-DC converter internal to an offshore wind farm

K. Musasa, M. N. Gitau, R. Bansal

Department of Electrical, Electronics and Computer Engineering, University of Pretoria, South Africa
Kabeyamusasa@gmail.com, njoroge.gitau@up.ac.za, rcbansal@ieee.org

Keywords: Active rectifier, DC-DC converter, small signal analysis, offshore wind park.

Abstract

This paper investigates the dynamic performance of an active rectifier integrated into a wind park. The small changes in the DC current and the DC voltage are examined. The small variations are caused by the miniature power flow unbalance between the offshore wind park and the grid land. Internal DC collector is considered into the wind park, which provides an internal DC medium voltage bus. The AC output signal from the wind generator to the internal DC collector or DC bus is regulated through active rectifier. An active rectifier is a cascade connection of an uncontrolled full bridge diode rectifier and a controlled DC-DC boost converter. The small changes in the DC current and DC voltage due to power flow unbalance are analysed across the boost converter. The way in which these small variations affect the internal medium DC voltage is determined. The results are presented in the form of small signal transfer functions and are evaluated with MATLAB software.

1 Introduction

The traditional topological structure of wind farms (WF) are based on internal AC links connections. With the recent advancement in DC technology, it has been found more efficient to use DC links than the AC system [1]. For the offshore wind farms, the weights of the equipment are severely reduced when DC links are employed. Most of the offshore wind farms (OWFs) are constructed far away from the land grid or load centre. Because of the higher charging currents in the AC cables, the DC cable becomes more preferable for power transmission. Large numbers of existing OWFs-based DC links use the line commutated converter (LCC) configurations. The LCC-DC converter consists of thyristors with firing angle control. The thyristors control commutations relay on the AC network. Thus, it has been found vulnerable to operate the LCC-DC converter within a weak AC network [2]. The short circuit ratio (SCR), which is the ratio between the short circuit levels or apparent power and the DC power, has to be maintained higher at the AC/LCC-DC junctions, at about the value of 3 for a high SCR or 2 for a critical SCR [3, 4]. In order to maintain the AC/DC link strong or with an acceptable SCR, the reactive power compensator and voltage-dependent current order limit (VDCOL) are installed in the AC/LCC-DC junction [2]. The SCR is directly proportional to the square of the AC voltage, and inversely proportional to the DC power. The reactive power compensator regulates the AC input voltage to the LCC converter. The VDCOL limits the DC current or DC power which flows through the DC line. The harmonic distortions generation by the LCC system is higher requiring large filter [5]. Recently it has been found more attractive to use the voltage source converter (VSC) based on pulse width modulation (PWM) control system in the AC/DC links [6]; the junction becomes AC/VSC-DC rather than AC/LCC-DC. The VSC-DC system consists of self-controlled switches, e.g. IGBTs, GTOs. The operations of switches are coordinated by means of the PWM. These switches provide independent control of active and reactive power because the PWM operation is independent of AC network. The VSC-DC system may not require any reactive power compensators or any VDCOL. This system has a low rate in harmonics generation, just small filters are needed. The VSC-DC converter has the ability to sustain a weak AC network, which has a very low SCR, by independently regulating the AC voltage and active power [4, 5]. But the cost and losses of the VSC based PWM converters are higher compare to the LCC-DC system [7].

In an OWF, each wind energy conversion system (WECS) consists of a wind turbine (WT) including mechanical supporting structure, transmission part, generator e.g. synchronous or induction generator which can be double fed induction generator (DFIG), a 50 or 60 Hz transformer and AC cables. All together are connected to an internal AC collector. However, because of the number of benefits offered by the VSC-DC links, the internal layout of the OWF can better relay on VSC-DC links which use forced commutation switches. Therefore, each WECS is then connected to an internal DC collector through VSC-PWM converter. The use of DC collector internal to the OWF also can reduce the size and weight of the WECS [1, 6].

The active rectifier is used in this paper as a VSC-PWM option to provide regulation of the internal DC parameters (current, voltage) of the wind park. The advantage of this layout is that, the elaboration of control scheme in the turbine (mechanical part) and generator (electrical part) can be less complex compare to the AC layout. Also, the efficiency of this system is higher, which provide the ability to the WECS to capture the maximum wind resources at all time. By comparison with the conventional VSC full-bridge converter,

where two switches are conducting at every instant. The power loss due to switch conduction is double. But for the active rectifier, only a single switch conducts at every instant. The drawback of this configuration can be the higher cost.
In this paper, the performances analyses of active rectifier are investigated across the DC-DC boost converter. The small parameters variations due to small power flow unbalance between the wind park and the land grid are examined. The rates of changes of parameters caused by the small variations are quantified. The results are presented in the form of loop transfer function and tested with MATLAB software.

2 System descriptions

An offshore wind park consists of a large number of wind energy conversion systems (WECS). The wind park is feeding a land grid through HVDC transmission system as shown in Figure 1. Each WECS consists of a turbine, a generator, a 50Hz transformer, and an active rectifier. An active rectifier is represented as a cascade connection of a full bridge diode rectifier and a DC-DC boost converter [8]. The structure of each WECS is as represented in Figure 2. The terminal of active rectifier is connected to an internal DC collector of the wind park.
The full bridge diode receives the AC signal to its input side. This is the output signal from the 50Hz transformer. The signal is then converted across the diode rectifier from AC signal to a no-controllable DC signal. The AC signal input-output to the transformer is also regulated across the wind generator. The DC-DC boost converter receives input as an uncontrollable DC signal. The no-controllable DC signal is then regulated through the DC-DC converter and PWM control to provide controllable parameters to the DC collector into the wind park. The standard for operating an HVDC grid is as described in [9].
The VSC-DC internal link of the wind park has the ability to capture the maximum power from the wind resources. This power is then sent to the land grid through the main DC collector and the HVDC line, as shown in the Figure 1. In order to understand the operation of VSC-PWM converter and its ability to track the maximum wind power [10-13]; referring to the basic power flow equation (1) and Figure 2 [8].

$$P = \frac{V_G V_C}{X_T} \sin\delta \qquad (1)$$

where V_G is the AC voltage at the generator side ; V_C is the AC voltage input to the bridge rectifier; X_T is the transformer impedance; and δ is the power angle which is the voltage phase difference between the generator and the input to the bridge rectifier, $\delta = \delta_C - \delta_G$, as shown in Figure 2. The voltage phase difference is associated to the frequency or speed of the generator. The maximum power tracking is attained by regulation of δ keeping about 90°. This is achieved by coordinating δ_C through the PWM control as according to equation (2) for a three phase system [12].

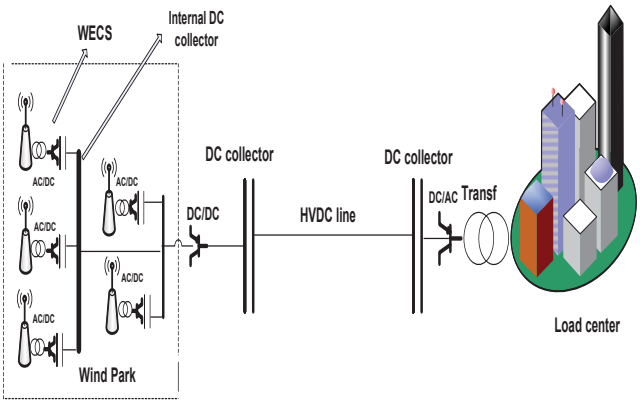

Figure 1: The grid system configuration

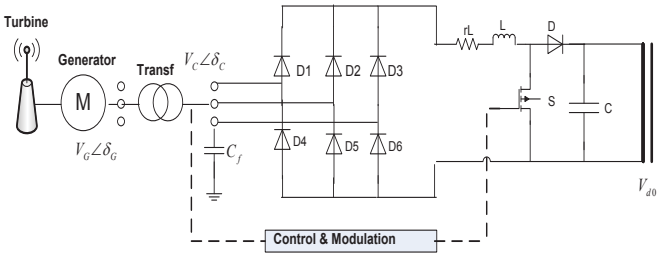

Figure 2: Wind energy conversion system

$$v_{sa}(t) = M\sin(\omega t + \delta_C)$$
$$v_{sb}(t) = M\sin(\omega t + \delta_C + 120^\circ) \qquad (2)$$
$$v_{sc}(t) = M\sin(\omega t + \delta_C + 240^\circ)$$

Where, M is the PWM modulation index; $v_{sa}(t)$, $v_{sb}(t)$, $v_{sc}(t)$ are the three phase AC voltage input to the VSC converter. The regulation of δ_C and M are realised through the control and modulation of the DC-DC boost converter as shown in Figure (2).
At the land grid-side either the LCC-DC or the VSC-DC inverter is considered in the DC/AC junction. In order to maintain the power flow balance, voltage regulator is installed into the receiving end to the land grid side [14]. For the power flow to be balanced, the total amount of power produced by the wind park has to be maintained equivalent to the power consumed to the land grid. If each individual WECS can capture a DC power of values P_{di} ; the total amount of power produced by the wind park P_d is equal to the sum of the individual captured DC power, equation (3).

$$P_d = \sum_{i=1}^{n} P_{di} \qquad (3)$$

Where n is the total number of WECS.
To balance the power flow between the wind park and the land grid, equation (4) has to be satisfied at all times.

$$P_d = P_{dR} \text{ or } V_{dS} I_d = V_{dR} I_d \qquad (4)$$

Where P_{dR} is the total power received into the land grid across the DC/AC junction; V_{dS} is the DC voltage at the sending end; P_d is the total power produced by the wind park; and I_d is the DC current flowing through the HVDC line. The system unbalance occurs when $P_d \neq P_{dR}$. The unbalance can cause the DC voltage V_{dS} of the main collector at the wind park side either to increase or decrease.

Different approaches have been proposed to maintain the power flow balance [15-17]. A voltage regulator was installed at the receiving end in the land grid. The voltage regulation process is defined in equation (5), and the voltage control loop is as presented in Figure (3) [17], S_R is a sensor proportional to the voltage-current relation.

The DC current I_d (or DC power P_{dR}) is controlled through the voltage regulator, equation (5).

$$I_d = K_V (V_{ref} - V_{dR}) \qquad (5)$$

Where V_{dR} is the actual or measured DC voltage in the receiving end; V_{ref} is the voltage reference in the receiving end; K_V can represent a system compensator. The DC voltage at the sending side is equal to the DC voltage at the receiving side plus the voltage drop through the HVDC line, as given by equation (6).

$$V_{dS} = V_{dR} + RI_d \qquad (6)$$

Where R is the resistance of the HVDC transmission line.

At the wind park side, voltage regulators are also integrated into each WECS to limit the current as proposed in [17].

In steady state grid operation, the installed voltage regulators does not regulating perfectly; thus, small power flow unbalances cannot be avoided. These small unbalances cause small variation in the system parameters (current, voltage, etc.) of the wind park.

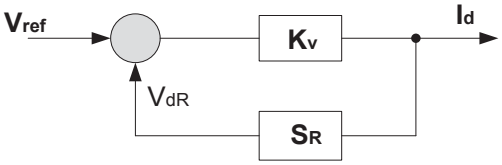

Figure 3: Voltage control loop

3 DC-DC converter

3.1 Dynamic model

For the design of an active rectifier, it is possible to use a full bridge diode rectifier in cascade with a step up DC-DC converter as shown in Figure 2 [8]. The DC voltage input to the DC-DC converter or output to the bridge rectifier is calculated as in equation (7) for a three phase and single bridge systems [18].

$$V_{dc} = \frac{3\sqrt{2}}{\pi} a_r V_s - \frac{3}{\pi} X_c I_{dc} \qquad (7)$$

Where, V_s is the line to line rms voltage; a_r is the converter transformer tap ratio; I_{dc} is the current which flow across the bridge rectifier; and X_c is the commutation reactance, it is equivalent to the transformer reactance X_t.

The equivalent circuit of DC-DC boost converter is as represented in Figure 4 [19]. The steady state or the average dynamic model is derived as given in equations (8) and (9) [19]. Some simplification is considered in the derivation of the transfer functions; the second order non-linear parameters are neglected.

$$L\frac{d\langle i_d(t)\rangle_{T_S}}{dt} = \langle v_{dc}(t)\rangle_{T_S} - r_L\langle i_{dc}(t)\rangle_{T_s} - V_{ce,sat}\rangle_{T_S}\langle m(t)\rangle_{T_S} + \left(1-\langle m(t)\rangle_{T_S}\right)\langle v_{dc}(t)\rangle_{T_s} - r_L\langle i_{dc}(t)\rangle_{T_s} - \langle v_{d0}(t)\rangle_{T_s} - V_{fwd}\rangle \qquad (8)$$

$$C\frac{d\langle v_{d0}(t)\rangle_{T_S}}{dt} = -\langle m(t)\rangle_{T_s}\frac{\langle v_{d0}(t)\rangle_{T_S}}{R_L} + \left(1-\langle m(t)\rangle_{T_s}\right)\left(\langle i_{dc}\rangle_{T_s} - \frac{\langle v_{d0}(t)\rangle_{T_s}}{R_L}\right) \qquad (9)$$

Where, $V_{ce,sat}$ is the voltage saturation or voltage drop across the switch; V_{fwd} is the forward voltage drop across the diode; r_L is the resistance across the inductor; R_L is the resistance of the DC collector; $\langle i_{dc}(t)\rangle$ is the average current flowing across the bridge rectifier; $\langle v_{d0}(t)\rangle$ is the average voltage output to the DC-DC converter, this is the internal voltage of the wind park or the internal DC voltage collector; $m(t)$ is the PWM modulation index, for a boost converter $m(t) = 1/(1-d(t))$; $d(t) = t_{on}/T_s$ is the duty ratio which is proportional to the AC voltage as according to equations (2) and (10); t_{on} is the interval of time when the switch is on; T_s is the switching period.

$$\langle d(t)\rangle_{T_s} = f\left(\langle v_{sabc}\rangle_{T_s}\right) \qquad (10)$$

The small signal models which give information on the dynamic of DC-DC boost converter are derived in equations (11) and (12). These are obtained by adding small signals to the averaging parameters as in equations (13), (14), (15), and (16).

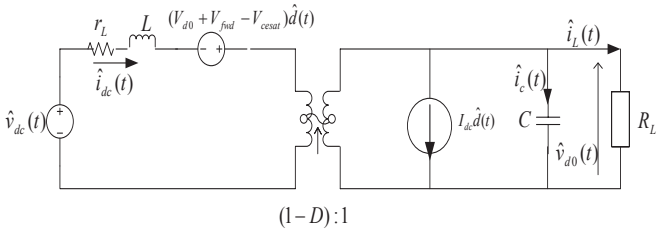

Figure 4: equivalent circuit of the boost converter

The small variations are caused by the spreading of small power flow unbalance into the grid.

$$L\frac{d\hat{i}_d(t)}{dt} = \hat{v}_{dc}(t) - r_L\hat{i}_{dc}(t) + \left(V_{d0} + V_{fwd} - V_{Cesat}\right)\hat{d}(t) - (1-D)\hat{v}_{d0} \qquad (11)$$

$$C\frac{d\hat{v}_{d0}(t)}{dt} = -\frac{\hat{v}_{d0}}{R_L} + (1-D)\hat{i}_{dc}(t) - I_{dc}\hat{d}(t) \quad (12)$$

$$\langle i_{dc}(t)\rangle = I_{dc} + \hat{i}_{dc} \quad (13)$$

$$\langle v_{dc}(t)\rangle = V_{dc} + \hat{v}_{dc} \quad (14)$$

$$\langle d(t)\rangle = D + \hat{d}(t) \quad (15)$$

$$\langle v_{d0}(t)\rangle = V_{d0} + \hat{v}_{d0}(t) \quad (16)$$

The symbol (^) stand for small signal parameters.

3.2 Transfer functions

In this paper, only the open loop transfer function is considered. In order to mitigate the small variations, a closed control loop system has to be implemented including the design of compensator system. This implementation is not part of this paper, it will be considered in our future study. From the two expressions, equations (11) and (12), the Laplace Transform is applied to derive the open loop transfer functions. The transfer function is the ratio between input and output signals. If considering G as an open loop transfer function of the DC-DC converter, its amplitude is used to quantify the rate in which the output signal change, when the input signal or control signal is subjected to small variations. In the dynamic model, the small signals consist of $\hat{v}_{dc}$ and $\hat{i}_{dc}(t)$ as inputs signals, $\hat{d}(t)$ as the control signal, and $\hat{v}_{d0}$ as the output signal to the DC-DC converter. The resulting open loop transfer functions are derived in equation (17), (18), (19), (20) and (21).

$$G_1(s) = \frac{\hat{v}_{d0}(s)}{\hat{v}_{dc}(s)} = \frac{(1-D)}{s^2LC + s\left(r_LC + \frac{L}{R_L}\right) + \frac{r_L}{R_L} + (1-D)} \quad (17)$$

$$G_2(s) = \frac{\hat{v}_{d0}(s)}{\hat{d}(s)} = \frac{-sI_{dc}L + (1-D)V_{d0} - r_LI_{dc}}{s^2LC + s\left(r_LC + \frac{L}{R_L}\right) + \frac{r_L}{R_L} + (1-D)} \quad (18)$$

$$G_3(s) = \frac{\hat{i}_{dc}(s)}{\hat{v}_{dc}(s)} = \frac{sC + \frac{1}{R_L}}{s^2LC + s\left(r_LC + \frac{L}{R_L}\right) + \frac{r_L}{R_L} + (1-D)} \quad (19)$$

$$G_4(s) = \frac{\hat{i}_{dc}(s)}{\hat{d}(s)} = \frac{sV_{d0}C + (1-D)I_{dc} + I_L}{s^2LC + s\left(r_LC + \frac{L}{R_L}\right) + \frac{r_L}{R_L} + (1-D)} \quad (20)$$

$$G_5(s) = \frac{\hat{v}_{d0}(s)}{\hat{i}_{dc}(s)} = \frac{(1-D)}{sC + \frac{1}{R_L}} \quad (21)$$

Where L and C are respectively the inductor and the capacitor internal network components of the DC-DC converter. The amplitudes of transfer functions are determined in the frequency domain. The small variations can be recorded online through digital monitoring system installed in each substation, e.g. the Digital Fault Recorder (DFR) or the phasor measurement units (PMU) [20].

4 Sample network description

The considered wind generator is a three phase system with 1 MW and 33 kV. The input voltage to the bridge rectifier is 66 kV, for a 1:2 transformer ratio. The DC output current I_{dc} to the bridge rectifier is calculated as in equation (22) [21].

$$I_{dc} = I_{srms} = I_1\sqrt{1 + THD_I^2} \quad (22)$$

I_{srms} is the rms AC supplied current; I_1 is the fundamental AC current which can be expressed as $I_1 = SCC/V_s$; SCC is the short circuit capacity (MVA); THD_I is the current total harmonic distortion given by equation (23) [21].

$$THD_I = \frac{1}{I_1}\sqrt{\sum_{h=2}^{\infty} I_h^2} \quad (23)$$

Where, I_h is the harmonic current components recorded at the input side of active rectifier. The SCC is the ratio between the active power P and the power factor PF in the AC/DC junction. The power factor is as expressed in equation (24) [21].

$$PF = \frac{1}{\sqrt{1 + THD_I^2}}\,DPF \quad (24)$$

Where, the displacement power factor DPF is about equal to 1. The active rectifier generates less harmonic distortion compare to the LCC converter. Thus, it is assumed in this paper a THD_I of about 15%. The transformer reactance $X_t = X_c$ is considered about 40% of the rated impedance $Z_{rated} = V_s / I_{1rms}$. The DC voltage V_{dc} output to the bridge rectifier is obtained as in equation (7).

The component networks of the DC-DC converter are seized according to equations (25) and (26).

$$L = \frac{(V_{dc} - r_LI_{dc} - V_{ce,sat})DT_s}{\Delta i_{pk-pk}} \quad (25)$$

$$C = \frac{I_LDT_s}{\Delta v_{pk-pk}} \quad (26)$$

Δi_{pk-pk} and Δv_{pk-pk} are respectively the peak to peak ripple current and voltage; V_{d0} is the voltage of the internal DC collector; I_L is the current which flows through the DC collector, this is calculated according to equation (27). The ripple current and voltage are considered low because of

presence of the active rectifier, $\Delta i_{pk-pk} < 0.2 I_{dc}$ and $\Delta v_{pk-pk} < 0.02 V_{d0}$.

(25)

$$I_L = \sqrt{(1-D)^2 \left[I_{dc}^2 - \left(\frac{\Delta i_{pk-pk}}{2} \right)^2 \right]} \qquad (27)$$

The steady state voltage V_{d0} is related to the PWM modulation index as expressed in equation (28).

$$V_{d0} = M(t) \left[V_{dc} - r_L I_{dc} - V_{fwd} + \left(1 - \frac{1}{M(t)} \right) \left(V_{fwd} - V_{cesat} \right) \right] (28)$$

Where $M(t) = 1/(1-D)$ for a DC-DC boost converter. The switching frequency is considered equal to 20 kHz.

5 Discussion

The output voltage to the bridge rectifier is calculated from equation (7), $V_{dc} = 64kV$. The voltage internal to DC collector is fixed, $V_{d0} = 155kV$ [14]. The duty ratio is calculated from equation (28), $D = 0.6$. There are established methods which can be used to estimate the $V_{ce,sat}$, V_{fwd}, and r_L. In this paper, an ideal system is considered, the power losses are neglected in the analyses. The components network of the DC-DC converter are calculated based on equations (25) and (26), $L = 640\mu H$ and $C = 58.1\mu F$. The open loop transfer functions waveforms for $G_1(s)$, $G_2(s)$, $G_3(s)$, $G_4(s)$ and $G_5(s)$ are plotted respectively in Figures (5), (6), (7), (8) and (9).

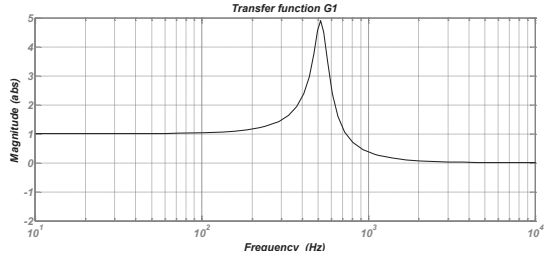

Figure 5: Transfer function of $G_1(s)$

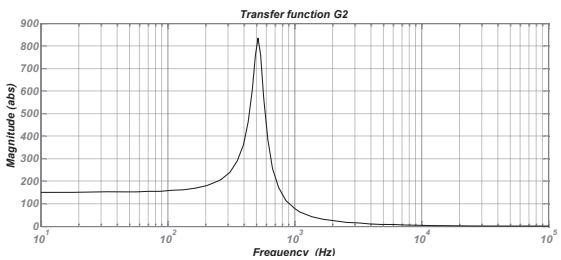

Figure 6: Transfer function of $G_2(s)$

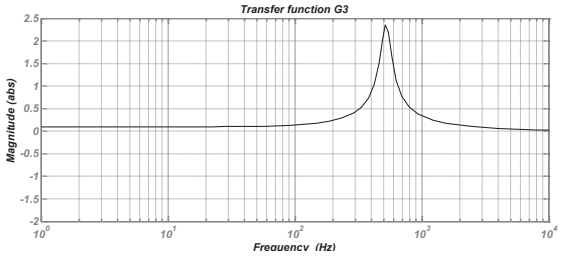

Figure 7: Transfer function of $G_3(s)$

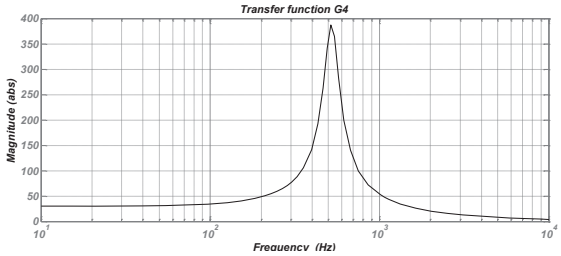

Figure 8: Transfer function of $G_4(s)$

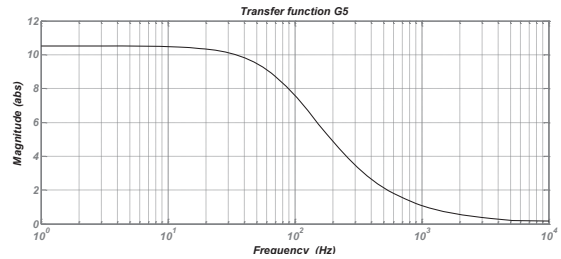

Figure 9: Transfer function of $G_5(s)$

It is noticed from the transfer functions that the rate of disturbances amplification is higher at the frequency lesser than the switching frequency. There is also a peak resonant which occurs at the frequency of 500 Hz for the TF $G_1(s)$, $G_2(s)$, $G_3(s)$, and $G_4(s)$. A filter can be designed and sampled at 500 Hz in order to withdraw this high amplitude of variations.

At the switching frequency ($f_s = 20kHz$) which is the steady state operating point, the amplitudes of variations are recorded as follows: $|G_1(s)|_{f_s} \approx 0.1$, $|G_2(s)|_{f_s} \approx 4.2$, $|G_3(s)|_{f_s} \approx 0.025$, $|G_4(s)|_{f_s} \approx 4.5$, and $|G_5(s)|_{f_s} \approx 0.112$. The rate of signal amplification is very higher for the TF $G_2(s)$ and $G_4(s)$. These two TFs links the $\hat{i}_{dc}(t)$ and the $\hat{v}_{d0}(t)$ to the $\hat{d}(t)$. Because $\hat{d}(t) = f(\hat{v}_{sabc}(t))$, the variations in the AC voltage input to the active rectifier have to be well controlled. The $\hat{i}_{dc}(t)$ and $\hat{v}_{d0}(t)$ will have an higher amplitude for just a small variation of the $v_{sabc}(t)$. However, a closed loop and compensator systems can be implemented to mitigate the higher variations.

The small signals parameters can be monitored by means of the digital monitoring units installed in each substation. It is also noticed in Figure (9) that the small variations are very

highly amplified when the switch operates at the frequency lower than the required switching frequency. At the high frequencies, the small signals are less amplified. This proves the reason why the VSC converter generate less distortion compare to the LCC converter, because of the high switching frequency operation of the VSC-PWM system.

6 Conclusion

This paper derives the model of an active rectifier. The small variations of parameters which occur into a wind park are quantified. The analyses are based on the DC-DC boost converter, which is an integrated part of the active rectifier. The active rectifier is installed into a wind park. The small variations of grid parameters are included in the model. These variations are caused by the small power flow unbalance between the wind park and the land grid. In order to determine the effect caused by these variations to the internal DC collector of the wind park; the open loop transfer functions of the DC-DC converter are derived. These transfer functions link all the necessary state variables of the grid to the internal DC collector. The steady state increase in the voltage at the DC collector internal to the wind park is quantified. The solution to mitigate these small variations can be achieved by means of an inner feedback current control loop and an outer feedback voltage control loop, including the current and voltage compensators implemented into the feedbacks. This control elaboration design will be part of our future study.

References

[1] C. J. Chou, Y. K. Wu, G. Y. Han, C. Y. Lee. "Comparative evaluation of the HVDC and HVAC links Integrated in a large offshore wind farm - an actual case study in Taiwan", *IEEE Trans. Ind. App*., vol. 48, no. 5, pp. 1639-1648, Sept./Oct. (2012).

[2] O. B. Nayak, A. M. Gole, D. G. Chapman, J. B. Davies. "Dynamic performance of static and synchronous compensators at an HVDC inverter bus in a very weak AC system", *IEEE Trans. Power Syst*., vol. 9, no. 3, pp. 1350-1358, Aug. (1994).

[3] A. Gavrilovic. "AC/DC system strength as indicated by short circuit ratios", *Int. Conf. on Trans. & Distr. Syst.*, UK., London, 17-20 Sept. (1991).

[4] J. Reeve, S.P. Lane-Smith. "Multi-infeed HVDC transient response and recovery strategies" *IEEE Trans. Power Del*., vol. 8, no. 4, pp. 1995-2001, Oct. (1993).

[5] B. R. Andersen, L. Xu. "Hybrid HVDC system for power transmission to island networks", *IEEE Trans. Power Del*., vol. 19, no. 4, pp. 1884-1890, Oct. (2004).

[6] N. Flourentzou, V. G. Agelidis, G. D. Demetriades. "VSC-Based HVDC power transmission systems: an overview", *IEEE Trans. Power Elect*, vol. 24, no. 3, pp. 592-602, March (2009).

[7] P. Bresesti, W. L. Kling, R. L. Hendriks, R. Vailati. "HVDC connection of offshore wind farms to the transmission system", *IEEE Trans. Eneg. Conv*., vol. 22, no. 1, pp. 37-43, March (2007).

[8] M. Liserre, F. Blaabjerg, Steffan Hansen. "Design and control of an *LCL*-filter-based three-phase active rectifier", IEEE Trans. Ind. Appl., vol. 41, no. 5, pp. 1281-1291, Sept./Oct. 2005.

[9] V. Akhmatov, M. Callavik, C.M. Franck, S. E. Rye, T. Ahndorf, M. K. Bucher, H. Müller, F. Schettler, R. Wiget. "Technical guidelines and prestandardization work for first HVDC grids", *IEEE Trans. Power Del*., vol. 29, no. 1, pp. 327-334, Feb. (2014).

[10] L. Guangkai, L. Gengyin, L. Haifeng, Z. C., Y. Ming. "Research on hybrid HVDC", *lnt. Conf. Power Sys. Tech.,* POWERCON Singapore, 21-24 Nov. (2004).

[11] W. Lu, B. T. Ooi. "Premium quality power park based on multi-terminal HVDC", *IEEE Trans. Power Del.*, vol. 20, no. 2, pp. 978-983, Ap. (2005).

[12] W. Lu, B. T. Ooi. "Optimal acquisition and aggregation of offshore wind power by multiterminal voltage-source HVDC", *IEEE Trans. Power Del*., vol. 18, no. 1, pp. 201-206, Jan. (2003).

[13] C. Du, E. Agneholm, G. Olsson. "Comparison of different frequency controllers for a VSC-HVDC supplied system", *IEEE Trans. Power Del*., vol. 23, no. 4, pp. 2224-2232, Oct. (2008).

[14] I. Erlich, Ch. Feltes, F. Shewarega. "Enhanced voltage drop control by VSC–HVDC systems for improving wind farm fault ridethrough capability", *IEEE Trans. Power Del.*, vol. 29, no. 1, pp. 378-385, Feb. (2014).

[15] M. Baradar, M. Ghandhari. "A multi-option unified power flow approach for hybrid AC/DC grids incorporating multi-terminal VSC-HVDC", *IEEE Trans. Power Sys.,* vol. 28, no. 3, pp. 2376-2383, August (2013).

[16] A. K. Marten, D. Westermann. "Power flow participation by an embedded HVDC grid in an interconnected power system", *3rd IEEE PES Innovative Smart Grid Technologies Europe (ISGT Europe),* Berlin, (2012).

[17] B. Silva, C. L. Moreira, H. Leite, J. A. P. Lopes. "Control strategies for AC fault ride through in multiterminal HVDC grids", *IEEE Trans. Power Del*., vol. 29, no. 1, pp. 395-405, Feb. (2014).

[18] N. Mohan, T. M. Undeland, W. P. Robbins. "Power electronics: converters, applications, and design", John Wiley & Sons, Inc., Third Ed, (2003).

[19] Erickson, Robert W. Fundamentals of Power Electronics. Second Ed. Secaucus, NJ, USA: Kluwer Academic Publishers, (2000).

[20] J. Pan, R. Nuqui, K. Srivastava, T. Jonsson, P. Holmberg, Y. J. Hafner. "AC Grid with Embedded VSC-HVDC for Secure and Efficient Power Delivery", *IEEE Energy conf.,* Atlanta, GA USA, 17-18 Nov. (2008).

[21] G. J. Wakileh. "Power System Harmonics, Fundamentals, Analysis and Filter Design", *Springer*, New York, (2001).